A novel bi-directional deformable fluid actuator

A novel bi-directional deformable fluid actuator

Carlo Ferraresi (corresponding author)
Department of Mechanical and Aerospace Engineering, Politecnico di Torino
C.so Duca degli Abruzzi 24, 10129 Torino, Italy
e-mail: carlo.ferraresi@polito.it
Walter Franco
Department of Mechanical and Aerospace Engineering, Politecnico di Torino
C.so Duca degli Abruzzi 24, 10129 Torino, Italy
e-mail: walter.franco@polito.it
Giuseppe Quaglia,
Department of Mechanical and Aerospace Engineering, Politecnico di Torino
C.so Duca degli Abruzzi 24, 10129 Torino, Italy
e-mail: giuseppe.quaglia@polito.it

Abstract

The deformable fluid actuators available on the market, i.e. pneumatic muscles and pneumatic springs, are designed to mainly exert compressive or tensile forces. This paper deals with a novel fluid deformable actuator, with three membranes, called *BiFAc3*, whose particular feature is the ability to exert both tensile and compressive forces. The structure of the actuator is based on three cylindrical coaxial non-isotropic membranes connected to two end plates, whose original shape allows the independent supply of the three internal

chambers. The first part of the paper deals with the internal structure and the geometry of the actuator, describes the operating principle and presents a prototype. The second part presents a modelling methodology that can be used to design and analyse the actuator in dynamic applications. The mathematical model of the actuator is based on three different levels of complexity which correspond to three consecutive design stages. The model has been experimentally validated: it is a useful tool for the choice of the actuator's geometrical dimensions, in order to satisfy specific applicative requirements.

Keywords: deformable fluid actuator, membrane actuator, pneumatic muscle, pneumatic spring, double effect deformable actuator

1. Introduction

The deformable fluid actuators available on the market can be grouped into two main categories: pneumatic muscles[1-11], which are designed to mainly exert tensile forces, and pneumatic springs[12-15], which are able to mainly exert compressive forces. They can be used in various applications that require the transmission of force between two mechanical elements in relative motion, and provide

typical advantages such as: low weight, high force/mass ratio, no sliding parts and therefore no need for lubrication, the use of cheap and non polluting fluids (oil free air, water), and the ability to drive structures that are kinematically non defined. On the other hand, the main limit of the currently available deformable actuators is their ability to exert either tensile or compressive forces.

The authors previously studied and developed a first prototype of a bi-directional deformable fluid actuator, with the aim of collecting the functionality of both a spring and a muscle in one actuator. That device, named *BiFAc2*[16], had two co-axial membranes and was able to exert both compressive and tensile forces , but showed limited compressive effectiveness.

The actuator described in this paper is an evolution of *BiFAc2*; it is in fact a bi-directional deformable fluid actuator that has three membranes, called *BiFAc3* (Figure 1), which presents improved compressive characteristics. The solution is original and has already been patented[17].

The operating principle of the actuator is described in the paper. An accurate dynamic modelling of the actuator is then proposed, with the aim of developing a useful tool for the dimensioning of the actuator, according to the requirements arising from a specific application. The mathematical model was then validated through a comparison with experiments performed on a prototype.

2. Structure and operating principle of the *BiFAc3* Actuator

BiFAc3 is made up of three coaxial cylindrical membranes, linked to two end plates, in such a way as to realize three coaxial sealed chambers (Figure 1 and Figure 2). The chambers are supplied by three separate ports R_c , R_i and R_e, which are located on the upper head (Figure 2). This allows the chambers to be supplied in an independent manner with three different pressures, indicated in Figure 2 as p_c, p_i and p_e.

In order to achieve the desired functionality, as will be explained later on, the three membranes must have a non-isotropic characteristic. In particular, from an ideal point of view, the central and external membranes should be inextensible in the longitudinal direction and infinitely compliant in the circumferential direction. The intermediate membrane instead should be inextensible in the circumferential direction and with no stiffness in the axial direction. It is possible to approach this condition by including properly oriented stiffening fibres in an elastomeric matrix. In our case, the deformable walls of the prototype have been made of a rubber membrane reinforced with plastic fibres oriented in a single direction. As can be seen in Figure 1, the fibres in the external and central mem-

branes are oriented in the longitudinal direction, while the fibres in the intermediate membrane are oriented in the circumferential direction.

BiFAc3 is the evolution of a previous, simpler bi-directional deformable actuator, *BiFAc2*, (Figure 3) which was realized with only two membranes, both ideally inextensible in the longitudinal direction and linked to two heads in such a way as to generate two co-axial sealed chambers[16]. Hereafter, a comparison of the functioning of both actuators will be given to explain the reasons that led the authors to develop the new solution.

The *BiFac3* actuator can operate in three basic configurations: *tension* mode, *compression A* mode and *compression B* mode (Figure 4).

The *tension* mode is realized by supplying both the intermediate and external chambers, and connecting the central chamber to the exhaust (Figure 4a). In this way, the fluid pressure exerts a radial force on both the central and the external membranes, which are stretched in the longitudinal direction. Such a stress is transmitted to the end plates, due to the presence of the fibres that have been inserted in the rubber matrix, thus determining a contraction of the actuator, i.e. the creation of a tensile force, like a pneumatic muscle and, in particular, a straight fibre pneumatic muscle[3]. If the pressure in the external chamber is equal to that in the intermediate chamber, the intermediate membrane becomes

irrelevant, and the actuator behaves in the same way as the two-membrane *BiFAc2* does, when only its external chamber is supplied. Unlike *BiFAc2*, in *BiFAc3* it is also possible to supply the intermediate chamber at a greater pressure than the one in the external chamber, since the intermediate membrane, being inextensible in the circumferential direction, can effectively separate the two chambers.

Compression B mode is achieved by supplying all three chambers (Figure 4c). Assuming that the pressure has the same value in all three chambers, the central and intermediate membranes would become irrelevant, and *BiFAc3* would behave exactly like a pneumatic spring, or like *BiFAc2* with both chambers being supplied at the same pressure. A typical drawback of both the pneumatic spring and *BiFAc2* in compression mode is that the pressure force exerted by the fluid on the end plates is rather limited, since it is partially balanced by the tensile force exerted by the external membrane. The third, intermediate membrane added to *BiFAc3* has been conceived to overcome such an inconvenience.

In this way, *BiFAc3* can operate in *compression A* mode, which is obtained by supplying both the central and intermediate chambers, and connecting the external one to the exhaust (Figure 3b). The intermediate membrane, which is circumferentially inextensible, maintains a cylindrical shape and ideally opposes

no resistance in the axial direction, thus allowing the actuator to lengthen freely, i.e. to exert a compressive force on the end plate that is proportional to the supply pressure, just like a normal pneumatic cylinder. This implies that, for equal geometrical and supply conditions, the compressive force is increased with respect to that produced by *BiFAc3* in *compression B* mode, or by *BiFAc2* with both chambers being supplied.

In short, *BiFAc3* is an actuator that is able to exert both tensile and compressive forces, the latter in two different modes, thus offering a large range for the force control. Its mechanical impedance is relatively low and could easily be controlled by varying the supply pressures in the chambers, as well as by providing controllable fluidic resistances between the chambers and possible auxiliary volumes. In this way the actuator acquires unique characteristics that may be exploited to control dynamic phenomena, such as shocks and vibrations.

The force F exerted by *BiFAc3* depends on a combination of factors, such as the internal chamber pressures, p_c, p_i, p_e, and the distance L between the end plates, as well as on the physical and geometric characteristics of the actuator itself. The following section reports a modelling methodology that allows the actuator force to be calculated as a function of the physical parameters and operating conditions, which can therefore be used as a design tool.

3. The Model

A mathematical model is an indispensable tool to achieve a correct design of the *BiFAc3* and to evaluate its actual performance in a defined application. Once the geometrical and physical data have been fixed, the model must be able to calculate the force F dynamically exerted by the actuator as a function of the supply pressures provided at the pneumatic ports on the end plates.

The model can be divided into two blocks, as depicted in Figure 5: the first one, called "supply dynamics", to evaluate the pressures inside the chambers; the second, called "force equilibrium", to calculate the force exerted by the actuator.

A particular problem arises by the peculiarity of the actuator, whose general performance is strictly related to few basic parameters, but can be drastically altered by the constructive details. To overcome this difficulty, it has been necessary to conceive a three-step design procedure, based on three different models of increasing complexity.

The first stage, named "*rapid design*", is made possible by a *simplified model*, and is aimed at individuating the two fundamental parameters of the actuator, i.e.

radius and length of membranes. These two values determine the basic actuator performances, i.e. the stroke and the static force.

Only at this point it is possible to complete a *detailed design* of the actuator, defining any parameter related to the necessary construction and mounting conditions. Obviously this may determine important variations on the device functionality with respect to what evaluated in the first stage. Such effects can be assessed by using a more accurate *ideal model*.

The third stage consists in the evaluation of performance provided by the actuator when it is employed in a defined application. This is made possible by a further model (*identified model*), which takes into account all actual characteristics of the actuator by means of a set of parameters, which can be identified through experimental measures, after the actuator has been constructed.

3.1 The *supply dynamics* block

This block calculates the chamber pressures, starting from the pressures at the supply ports. The block structure is shown in Figure 6. The symbols p_{sc}, p_{si} and p_{se} indicate the pressures which are applied upstream of the supply ports, for the central, intermediate and external chambers respectively; the internal pres-

sures of the actuator chambers are indicated with p_c, p_i and p_e for the central, intermediate and external chambers respectively (Figure 2).

The algorithm used to calculate the pressure is the same for the three chambers. The detailed block scheme pertaining to the external chamber is reported in Figure 6 as an example.

Once the geometry of the actuator has been defined, the *volume* block calculates the volume of chamber V_e as a function of distance L between the end plates, on the basis of some hypotheses that will be explained hereafter.

Given the pressure values at supply port P_{se} and inside chamber P_e, it is possible to calculate the air flow rate G_e that enters the chamber by means of the *flow equation* block. The following relations are consistent with the formulation defined in the ISO 6358 standard, considering the upstream temperature of air in standard conditions. The flow rate is considered positive when it enters the chamber. When $P_{se}>P_e$, two distinct cases are possible:

for $b_e < \frac{P_e}{P_{se}} < 1$, corresponding to the subsonic condition:

$$G_e = \rho_N \cdot C_e \cdot P_{se} \sqrt{1 - \left(\frac{P_e / P_{se} - b_e}{1 - b_e} \right)^2} \qquad (1)$$

while for $\frac{P_e}{P_{se}} < b_e$, i.e. in the case of sonic nozzle:

$$G_e = \rho_N \cdot C_e \cdot P_{se} \qquad (2)$$

Vice versa, when $P_e > P_{se}$, the flow is discharged from the chamber and therefore negative. Two cases are again possible:

for $1 < \frac{P_e}{P_{se}} < \frac{1}{b_e}$, corresponding to the subsonic condition:

$$G_e = -\rho_N \cdot C_e \cdot P_e \sqrt{1 - \left(\frac{P_{se} / P_e - b_e}{1 - b_e} \right)^2} \qquad (3)$$

while for $\frac{P_e}{P_{se}} > \frac{1}{b_e}$,

$$G_e = -\rho_N \cdot C_e \cdot P_e \tag{4}$$

The *continuity equation* block, indicated in Figure 6, calculates the pressure gradient inside the variable volume chamber. Assuming a polytrophic process, defined by an appropriate value of the coefficient γ:

$$\dot{P}_e = \frac{\gamma R_G T_0}{V_e(L)} \left(\frac{P_e}{P_{0e}} \right)^{\frac{\gamma-1}{\gamma}} G_e - \frac{\gamma P_e}{V_e(L)} \dot{V}_e(L) \tag{5}$$

allows one to calculate the derivative of the absolute pressure P_e in the external chamber, which may be integrated in order to obtain the dynamic value of the pressure. Through analogous procedures, it is possible to determine the trend of the absolute pressures in the remaining chambers, P_c and P_i . The relative pressures p_c, p_i and p_e can easily be calculated from the three absolute pressures.

3.2 The *force equilibrium* block

This block calculates the force F exerted by *BiFAc3* as a function of the relative pressures inside the chambers (central p_c, intermediate p_i and external p_e) and of the distance L between the end plates.

As described before, three different models, with increasing complexity, are necessary to design the actuator and accurately evaluate its performance (Figure 7): a *simplified* model with an elementary geometry; an *ideal* model, which takes into account the actual geometry of the actuator membranes, but neglects the assembly imperfections and the membrane stiffness; an *identified* model, which considers both the assembly errors and the membrane stiffness by means of parameters which can be determined through static tests conducted on the real actuator.

All three models have been developed under the following hypotheses:

1. the central and external membranes are considered inextensible in the longitudinal direction and fully compliant in the circumferential direction;
2. the longitudinal section of the central and external membranes is shaped as a circumference arc, for each working position, with variable curvature radius R and fixed length L_f (Figures 8 and 14);

3. the intermediate membrane is considered to be fully compliant in the axial direction and inextensible in the circumferential direction; this assumption makes sense when the pressure in the intermediate chamber is greater or equal to that in the external chamber; in this case, the intermediate membrane behaves like a bellows, and the axial force exerted is negligible compared to those of the external and central membranes, as confirmed by experimental tests; vice versa, if the pressure in the external chamber is greater than the one in the intermediate chamber, the membrane collapses and the assumption loses validity;
4. the equivalent force F_m acting on a membrane (central or external) can be calculated by transforming its axial-symmetric closed structure into a surface with the same longitudinal profile, as depicted in Figure 9, and writing the equilibrium equation of the membrane.

Considering hypotheses 1 and 2, with reference to Figure 8, and using the auxiliary angle ϕ, it is possible to write:

$$\begin{cases} R \cdot 2\phi = L_f \\ R \cdot \sin\phi = L/2 \end{cases} \tag{6}$$

and obtain:

$$\frac{L}{L_f} = \frac{sin\phi}{\phi} \tag{7}$$

Once the length of the fibres L_f has been chosen according to specific design requirements , equation (7) represents the relation between the actuator length L and an auxiliary angle ϕ. Since the equation cannot be inverted analytically, function $\phi = \phi(L)$ has been derived numerically.

Δp being the pressure drop between the internal and external surface of the membrane (this equation is valid for the membranes that are inextensible in the longitudinal direction, i.e. the central and external membranes), the horizontal force equilibrium (Figure 9, left) allows one to calculate the total equivalent force acting on the membrane:

$$F_m = \frac{L \cdot \pi \cdot r}{sin\phi} \Delta p \tag{8}$$

Projecting such a force in the axial direction, and bearing in mind equation (7), the axial component can be obtained:

$$F_{ma} = \pi \cdot r \cdot L_f \frac{\cos\phi(L)}{\phi(L)} \Delta p \tag{9}$$

Pressure resultant F_p on the end plate is equal to:

$$F_p = \pi \cdot \left[r_c^2 \cdot p_c + \left(r_i^2 - r_c^2 \right) \cdot p_i + \left(r_e^2 - r_i^2 \right) \cdot p_e \right] \tag{10}$$

The value of the total force exerted by the actuator can therefore be calculated from the axial equilibrium equation of one end plate. With reference to Figure 9, one obtains:

$$F = F_{mea} + F_{mca} - F_p \tag{11}$$

where F_{mea} and F_{mca} are the axial forces acting on the external and central membranes, respectively.

The following sections describe the *simplified* and the *ideal* models. The prototype and the experimental tests are then presented. Finally, the *identified* model is described.

4. The *Simplified* Model

This model has a simplified geometry, i.e. that of an actuator in which the connection radius of all three membranes is equal to r and the axial length of all the membranes is equal to L_f (Figure 8). Under these hypotheses, equation (11) becomes:

$$F = \pi \cdot r \cdot L_f \frac{\cos(\phi(L))}{\phi(L)}(p_e + p_i - p_c) - \pi \cdot r^2 p_c \qquad (12)$$

Equation (12) may be used to derive the static dimensionless characteristic in the three main operating modes of the actuator, which were previously introduced and defined as *tension*, *compression A* and *compression B*. The dimensionless representation allows one to neglect the actuator size. Moreover, the effect of the proportions on the static actuator performance may be highlighted by introducing the slimness coefficient $\delta = L_f/r$ and the plate area $A = \pi r^2$.

From equation (12), it is possible to obtain:

- the *tension* static characteristic ($p_e=p_i=p$, $p_c=0$)

$$\frac{F}{p \cdot A} = \frac{F}{\pi \cdot r^2 p} = 2\delta \frac{\cos(\phi(L))}{\phi(L)} \tag{13}$$

- the *compression A* static characteristic ($p_c=p_i=p$, $p_e=0$)

$$\frac{F}{p \cdot A} = -1 \tag{14}$$

- the *compression B* static characteristic ($p_c=p_i= p_e=p$)

$$\frac{F}{p \cdot A} = \delta \frac{\cos(\phi(L))}{\phi(L)} - 1 \tag{15}$$

The graphs of the static characteristics provided by equations (13-15) are shown in dimensionless form in Figure 10, with the slimness factor $\delta=L_F/r$ as the curve parameter. The tension force is positive and the compression force is negative

for the assumed reference system. One can observe that a slimmer actuator is able to exert higher tension forces, since it is able to produce a higher positive force at the same contraction ratio.

5. The *Ideal* Model

The ideal model considers the three membranes to have different connection radiuses to the end plate ($r_e \neq r_i \neq r_c$) and the central and external membranes to have different fibre lengths ($L_{fe} \neq L_{fc}$). Therefore, considering the geometrical differences of the membranes, equations (9) and (10), substituted in (11), produce the following expression:

$$F = \pi \cdot \left\{ r_e \cdot L_{fe} \frac{\cos(\phi_e(L))}{\phi_e(L)} p_e + r_c \cdot L_{fc} \frac{\cos(\phi_c(L))}{\phi_c(L)} (p_i - p_c) - \left[r_c^2 \cdot p_c + \cdot (r_i^2 - r_c^2) \cdot p_i + \cdot (r_e^2 - r_i^2) \cdot p_e \right] \right\} \quad (16)$$

The ideal model is able to highlight several effects on performance due to the actuator geometry, which are particularly evident in the case in which the actuator is used in *tension mode*, i.e. at ($p_e=p_i=p$, $p_c=0$). Moreover, posing:

$L_{fe}=L_{fc}=L_f$; $r_e=r$, $\Delta r= r_e-r_c$

equation (16) simplifies to:

$$\frac{F}{p \cdot A} = \left(2 - \frac{\Delta r}{r}\right) \cdot \left(\delta \frac{\cos(\phi(L))}{\phi(L)} - \frac{\Delta r}{r}\right) \tag{17}$$

Two extreme cases can be individuated in equation (17): $\Delta r/r=0$, when the *tension* mode of the simplified model (i.e. equation (13)) is again met, and $\Delta r/r=1$, when the central membrane has no influence ($r_c=0$) and the *compression B* mode of the simplified model (equation (15)) is reached. The graph in Figure 11 shows the trend of equation (17) for an actuator with a slimness ratio δ=1. It is clear that, as Δr rises, the effectiveness of tension is reduced, because the resultant of pressure on the annular surface between the external and central membrane opposes the tensile force exerted on the plate by the membranes. Moreover, the available contraction stroke is also reduced (such a stroke is obtained by measuring the range of L/L_f in which $F/(pA)>0$).

6. The Prototype: Experimental Tests and *Identified* Model

The prototype shown in Figure 12 has been realized in order to experimentally verify the innovative behaviour of the *BiFAc3* actuator. A cross-section of the prototype is depicted in Figure 13, where it is possible to see how the membranes are mounted onto the heads. The conical coupling between the membranes and head surfaces eliminates any leakage, while an independent chamber supply is made possible due to the special configuration of the passageways on the upper head. The threaded holes in the centre of the heads allow more actuators to be serially connected, thus producing systems with enhanced stroke capability.

The static characterization of the actuator has been carried out on a proper test bench. The relative position of the heads was controlled by a hydraulic servo-actuator, while the pressures inside the three chambers were regulated to constant preset values by means of proportional pneumatic valves. The distance between the heads was read by a LVDT (F.S. 200 mm, linearity 1% F.S.), while the load applied to the actuator was measured by means of a load cell (F.S. 5000 N, linearity 0.05 % F.S.).

The performances of actuators with different slimness ratio δ have been tested to obtain the static characteristic of the actuator, i.e. $F=F(L, p_e, p_i, p_c)$, which can be compared with the theoretical values provided by equations (12) or (16) of the models. The experimental results shown hereafter are related to a *BiFAc3* actuator which has the following geometrical parameters: r_e=0.0658 m, r_i=0.0601 m, r_c=0.0501 m, $L_{fe}=L_{fc}$=0.0856 m, $\delta=L_{fc}/r_e$=1.3. The tensile stroke of the prototype was of about 15 mm.

A first analysis of the experimental results has highlighted that the ideal model, as expressed by equation (16), shows some inaccuracy in the performance evaluation, since it neglects two main phenomena: the energy absorbed to stretch the membrane rubber in the circumferential direction, and the difference between the actual shape of the deformed membranes and the theoretical one, which disproves the initial assumption of bi-univocal relationship between the connection angle of the membranes and the working position (Figure 14). These two inaccuracies can be compensated by introducing corrective terms, which can be deduced from the experimental data, into the model. The resistance of the membranes to the deformation is represented by the force:

$$F_k = k\left(L - L_f + c_m\right) \tag{18}$$

where:

- k is the axial stiffness of the set of three membranes, expressed in N/m; it has been measured compressing the actuator with chambers connected to exhaust;
- L_f-c_m is the working position at which the measured compressive force is equal to that expressed by the identified model.

The inaccuracy due to the connection angle of the central and external membranes can be corrected by adopting appropriate coefficients that must be added to the values calculated through equation (7). The correct angles of the central and external membranes become:

$$\phi_{cc} = \phi_c(L) + c_c \tag{19}$$

$$\phi_{ec} = \phi_e(L) + c_e \tag{20}$$

where c_c and c_e are the mean errors estimated in the evaluation of the connection angles of the central and external membranes, respectively.

c_e has been identified comparing the force calculated by the *ideal model* with the one generated by the prototype in *compression B* mode; c_c has been identified comparing the force calculated by the *identified model* (imposing c_c equal to 0) with the one generated by the prototype in *tension mode*.

The total actuator force, as calculated by the *identified model*, is obtained from the sum of the forces exerted by the external and central membranes (equation (9) using (7), (19), (20)), and from the pressure (equation (10)) as for the ideal model; but the effect of the axial stiffness must also be added, as per equation (18), thus obtaining:

$$F = F_{mea} + F_{mca} - F_p + F_k \tag{21}$$

The static characteristic expressed by (21), for a *BiFAc3* actuator with the previously defined geometry, is presented in Figure 15, considering the following experimental coefficients: k=7800 N/m; c_m=5 mm; c_e=6.5 deg; c_c=13 deg.

A comparison between the experimental results and the identified model is shown in Figure 16. The good forecasting capability of the model is evident.

7. The dynamic response

The dynamic behaviour of the *BiFAc3* depends on both the characteristic of the supply section and the size of the actuator. In other words, for given values of the supply ports' pneumatic conductance, the dynamics is influenced by the chamber volumes, which vary in such a non linear way due to the membranes. The *identified model* is therefore the only tool able to perform a reliable dynamic simulation, allowing to evaluate the possible application of the actuator in a defined mechanical system.

Some simulations have been carried out in order to investigate the dynamic performance of the *BiFAc3*. By way of example, it has been possible to evaluate the actuator response to a step variation of the supply pressure from ambient value to 75 kPa. Table 1 reports the response times to reach the 99% of final steady force in all three operative configurations of the actuator, for three different actuator's height ratio L/L_f.

Table 1. Response time of the prototype *BiFAc3* to supply pressure step of 75 kPa

configuration	L/L_f=0.84	L/L_f=0.88	L/L_f=0.92

tensile	60 ms	56 ms	50 ms
compression A	43 ms	42 ms	41 ms
compression B	61 ms	57 ms	51 ms

8. Conclusions

BiFAc3 is a bi-directional deformable actuator with low mechanical impedance, which is able to exert both tensile and compressive forces. Its structure, comprising three coaxial membranes, allows the range of the compressive force to be extended, compared to *BiFAc2,* the actuator with only two membranes. In addition, the 3-membrane structure allows the actuator impedance to be dynamically controlled, as regards the stiffness and damping characteristics. This makes *BiFAc3* a device which may be effectively used in applications that require the control of dynamic phenomena, such as shocks and vibrations.

The prototypes that have been realized so far are still limited, as far as the pressure and force values are concerned; this is mainly due to difficulties in the construction of the membranes, which will soon be overcome due to cooperation

with a specialized company. However, the experimental tests have confirmed the expected performance of the device.

The design procedure proposed in this paper, which has been articulated in three subsequent stages, leads to the complete development of the device: in the first stage, the *simplified model* is used to identify the main geometrical proportions, according to a specified application; in the second stage, the actual dimensions of the device can be defined by means of the *ideal model*; finally, through an appropriate experimental identification of the physical characteristics of the device, the *identified model* will allow the actuator to be simulated in a very accurate way, thus allowing its effective integration in a given dynamically controlled mechanical system.

Acknowledgements

The authors would like to thank Mr. Manuele Musso for his cooperation in the realization of the prototype and in the running of the experimental tests.

Nomenclature

Symbol	Meaning	units
b	critical pressure ratio	
c	mean error of the membrane connection angle	rad
c_m	experimental corrective coefficient for the elastic force	m
k	axial stiffness of the actuator	N/m
p	relative pressure	Pa
r	connection radius of a membrane	m
A	end plate area	m^2
C	fluidic conductance	$m^3/(sPa)$
F	tensile force of the actuator	N
F_k	resistance of the membranes to deformation	N
F_m	force acting on the membrane	N
F_{mea}	axial component of the force acting on the external membrane	N
F_{mca}	axial component of the force acting on the central membrane	N
F_p	pressure force on the end plate	N
G	Mass flow rate	kg/s
L	height (length) of the actuator	m
L_f	length of one fibre in an axial section	m
P	absolute pressure	Pa
R	curvature radius of a membrane section	m
R_G	air constant	J/(kg K)

T	air temperature	K
V	volume of one actuator chamber	m^3
δ	$= L_f/r$ slimness ratio	
ϕ	auxiliary angle	rad
ϕ_{cc}	correct auxiliary angle of the central membrane	rad
ϕ_{ec}	correct auxiliary angle of the external membrane	rad
γ	polytrophic coefficient	
ρ_N	air density in standard conditions	kg/m^3

Subscripts	**Meaning**
e, i, c	external, intermediate, central
m	Membrane
a	Axial
f	Fibre
se, si, sc	external, intermediate, central supply
0	initial condition

Capital *P* refers to absolute pressure, and lower case *p* refers to relative pressure.

References

1. Tondu B. Modeling of the McKibben Artificial Muscle: a Review. *J. Intell. Mater. Syst. Struct.* 2012; 23(3): 225-253.

2. Chou C, Hannaford B. Measurement and Modeling of McKibben Pneumatic Artificial Muscles. *IEEE Trans. Robot. Automat.* 1996; 12(1): 90-102.
3. Ferraresi C. Franco W. Manuello Bertetto A. Flexible Pneumatic Actuators: A Comparison Between the McKibben and Straight Fibres Muscles. *J. Robot. Mechatron.* 2001; 13(1): 56-63.
4. Kothera C.S. Jangid M. Sirohi J., Wereley N.M. Experimental Characterization and Static Modeling of McKibben Actuators. *J Mech Des.* 2009; 131(9): 091010.
5. Schulte H.F. The characteristics of the McKibben artificial muscle. In: The Application of External Power in Prosthetics and Orthotics. Washington, DC, National Academy of Sciences, Appendix H, Publication 874, 961, pp.94–115.
6. Inoue K. Rubbertuators and Applications for Robots. In *4th Int. Symp. On Robotics Research*, Santa Cruz, USA, August 9-14 1987.
7. Caldwell D.G. Medrano-Cerda G.A. Goodwin M.J. Control of Pneumatic Muscle Actuators. *IEEE Control Syst. Mag.* 1995; 15(1): 40-48.
8. Tsagarakis N. Improved Modelling and Assessment of pneumatic Muscle Actuators. In: *International Conference on Robotics and Automation,* San Francisco, USA, 24-28 April 2000.

9. Immega G. Kukolj M. *Axially contractable actuator*. Patent 4,939,982, USA, 1990.
10. Yarlott J. M. *Fluid actuator*. Patent 3,645,173, USA, 1972.
11. Daerden F. Lefeber D. The concept and design of pleated pneumatic artificial muscles. *Int. J. Fluid Power* 2001; 2(3): 41–50.
12. Quaglia G. Sorli M. Air Suspension Dimensionless Analysis and Design Procedure. *Veh. Syst. Dyn.* 2001; 35(6): 443-475.
13. Lee S.J. Development and Analysis of an Air Spring Model. *Int. J. Automot. Technol.* 2010; 11(4): 471-479.
14. Ballo I. Technical Note: Properties of Air Spring as a Force Generator in Active Vibration Control Systems. *Veh. Syst. Dyn.* 2001; 35(1): 67-72.
15. Nieto A.J. Morales A.L. González A. Chicharro J.M. Pintado P. An analytical model of pneumatic suspensions based on an experimental characterization. *J. Sound Vib.* 2008; 313**(**1-2): 290-307.
16. Ferraresi C. Franco W. Quaglia G. Bi-Directional Flexible Pneumatic Actuator. In *Proceedings of the Fifth International Symposium Fluid Power*, Nara, Japan, 12-15 November 2002, pp. 25-30.
17. Ferraresi C. Franco W. Quaglia G. *Double Acting Deformable Fluid Actuator of the Muscle Type With Three Chambers*. Patent 7,770,508 B2, USA, 2010.

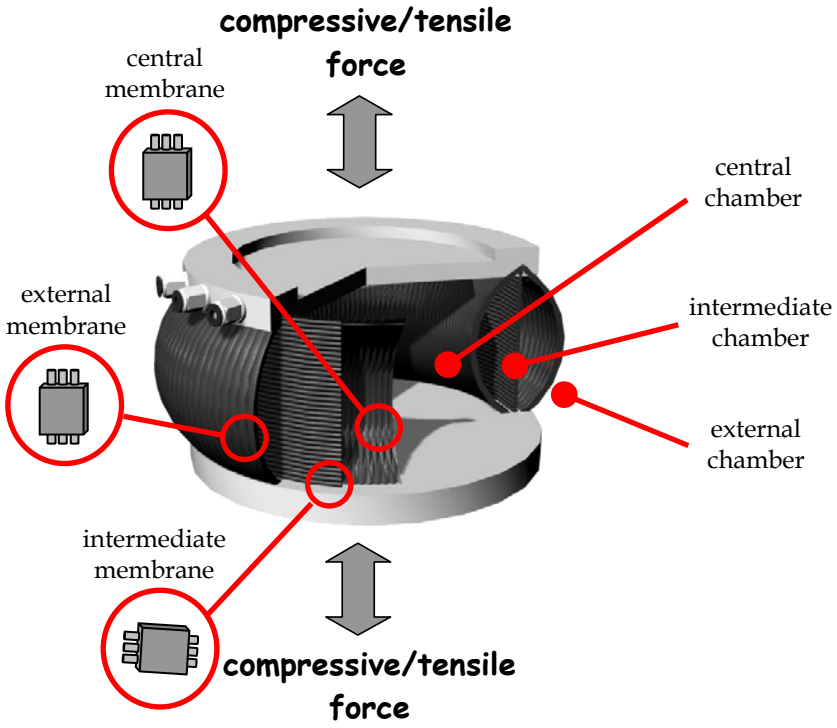

Figure 1. The *BiFAc3* actuator.

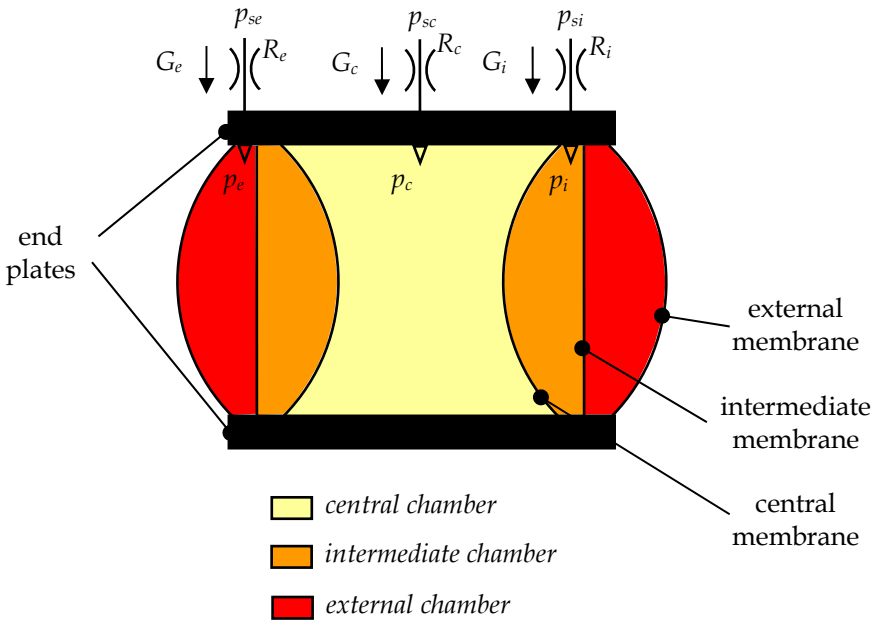

Figure 2. The *BiFAc3* scheme.

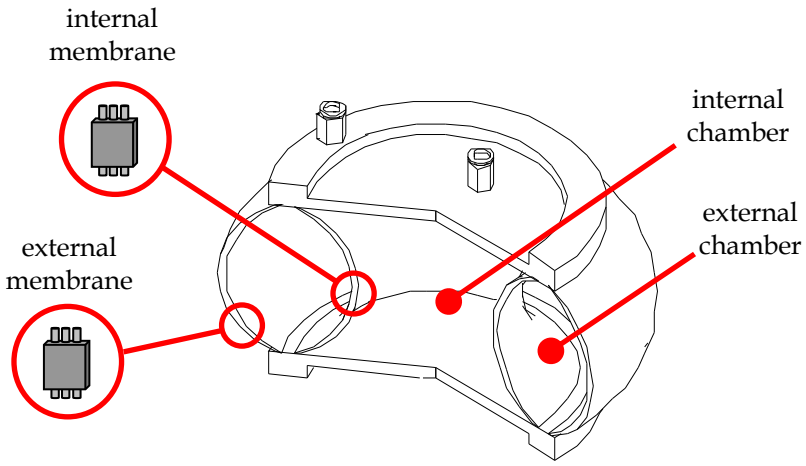

.

Figure 3. The *BiFAc2* section.

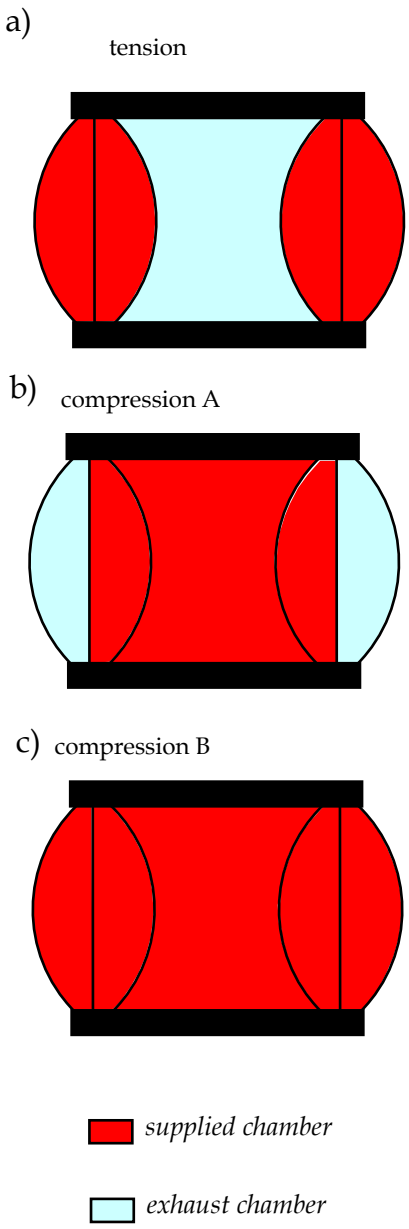

Figure 4. The *BiFAc3* operating conditions.

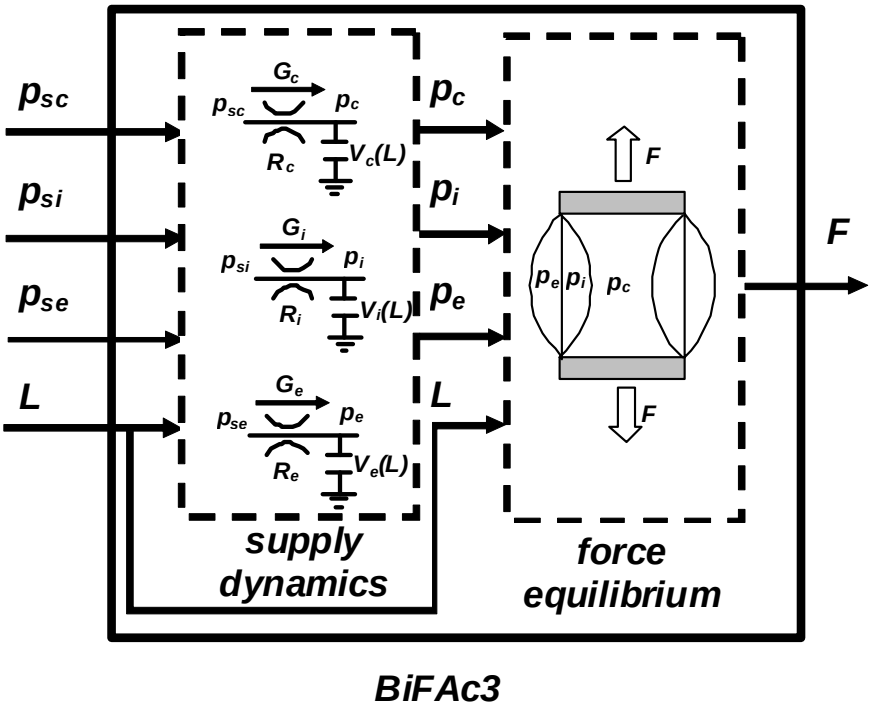

Figure 5. Block scheme of *BiFAc3*.

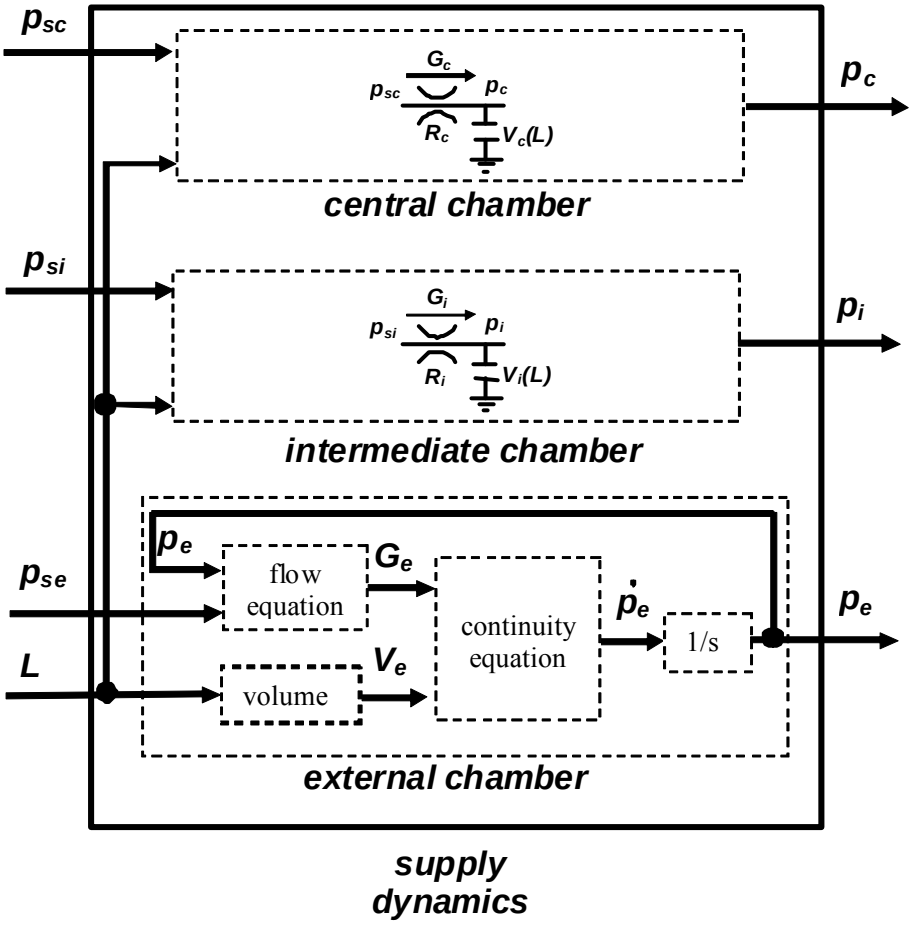

Figure 6. The *supply dynamics* block.

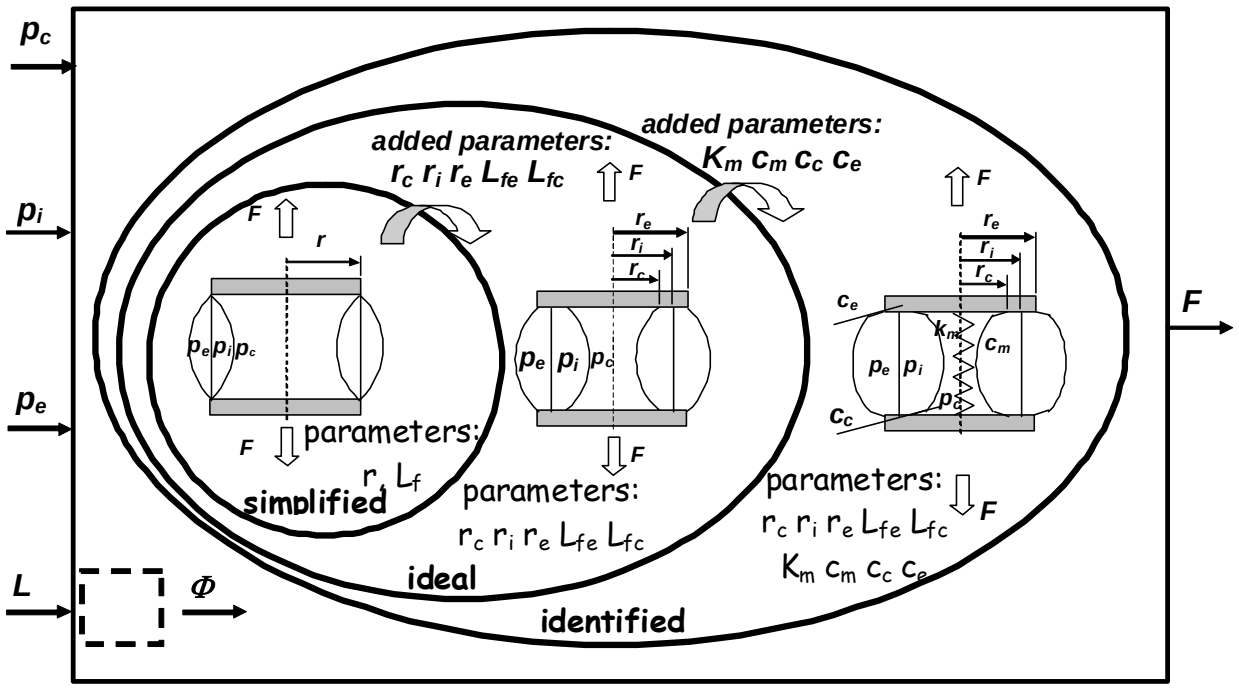

Figure 7. The three versions of the *force equilibrium* block: simplified, ideal, identified.

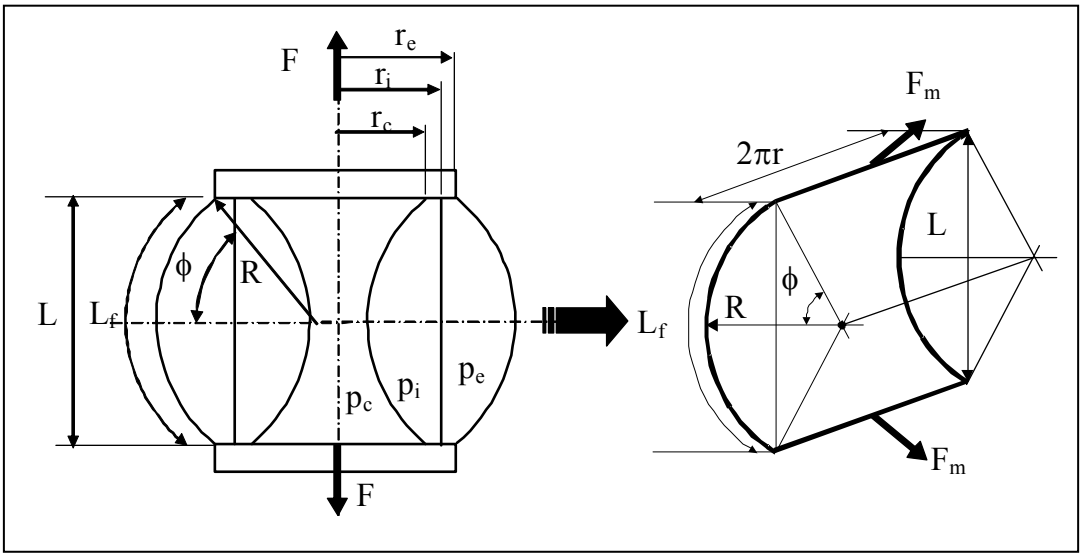

Figure 8. The actuator geometry.

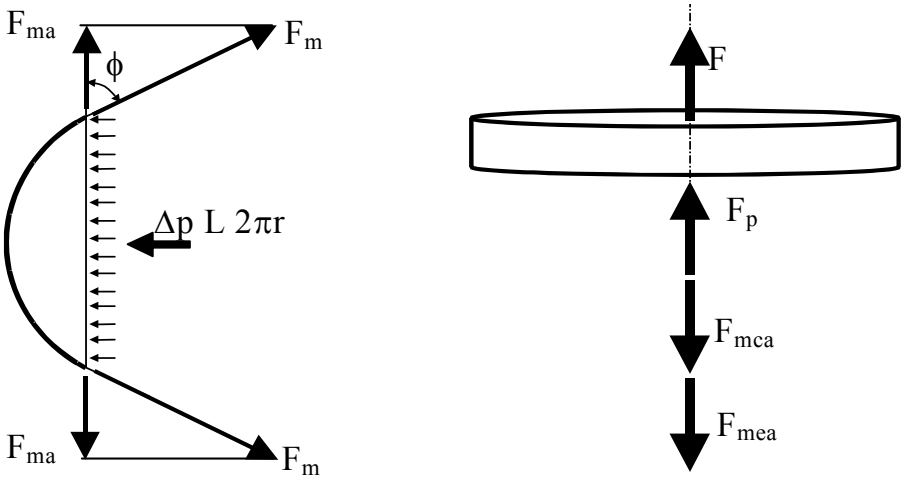

Figure 9. Equilibrium of one membrane and of the whole end plate.

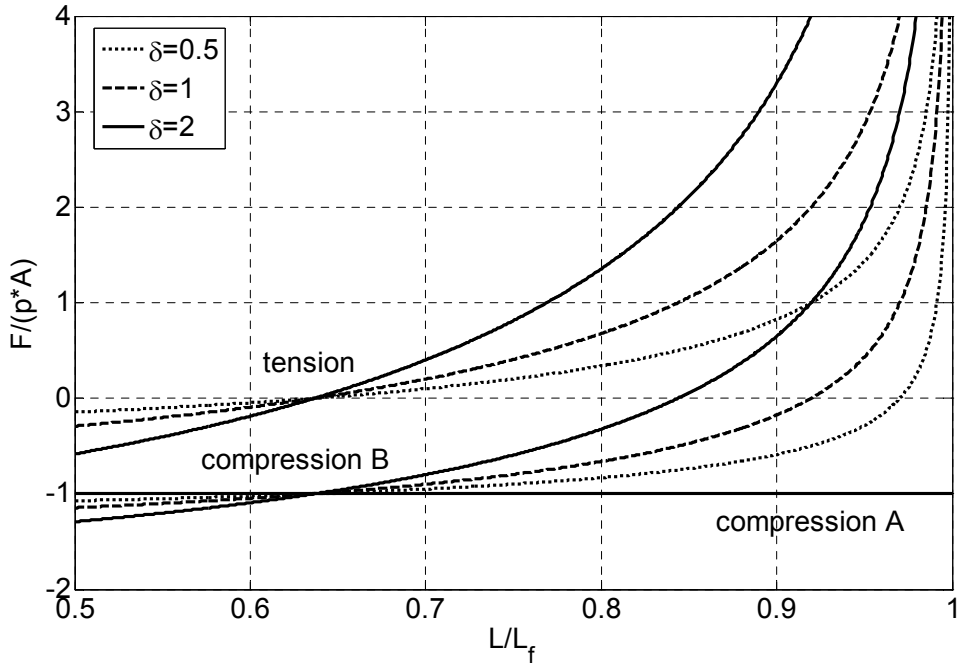

Figure 10. Static characteristic of the simplified model (parameter $\delta = L_F/r$).

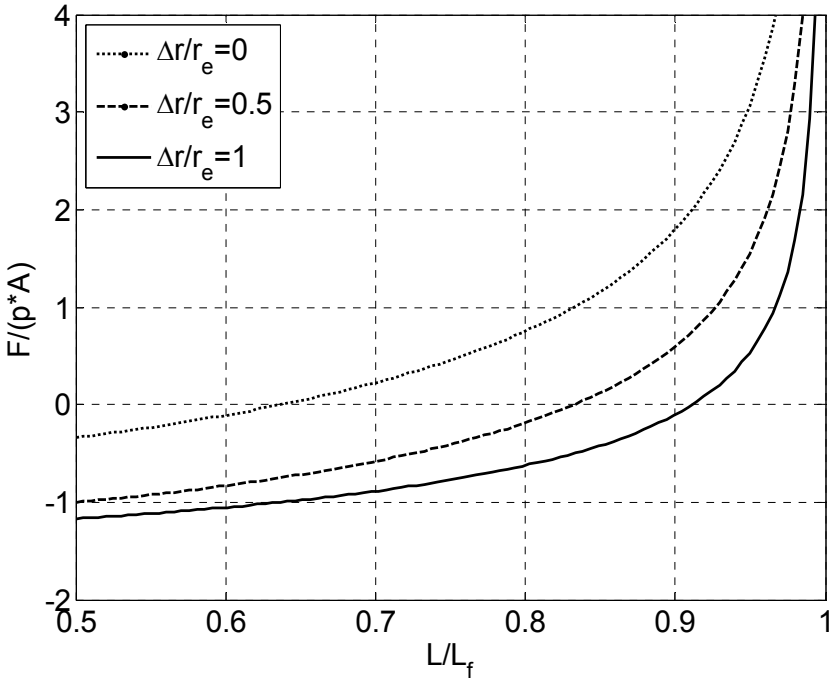

Figure 11. Static tension characteristic of the ideal model, $\delta=1$, parameter $\Delta r = r_e - r_c$.

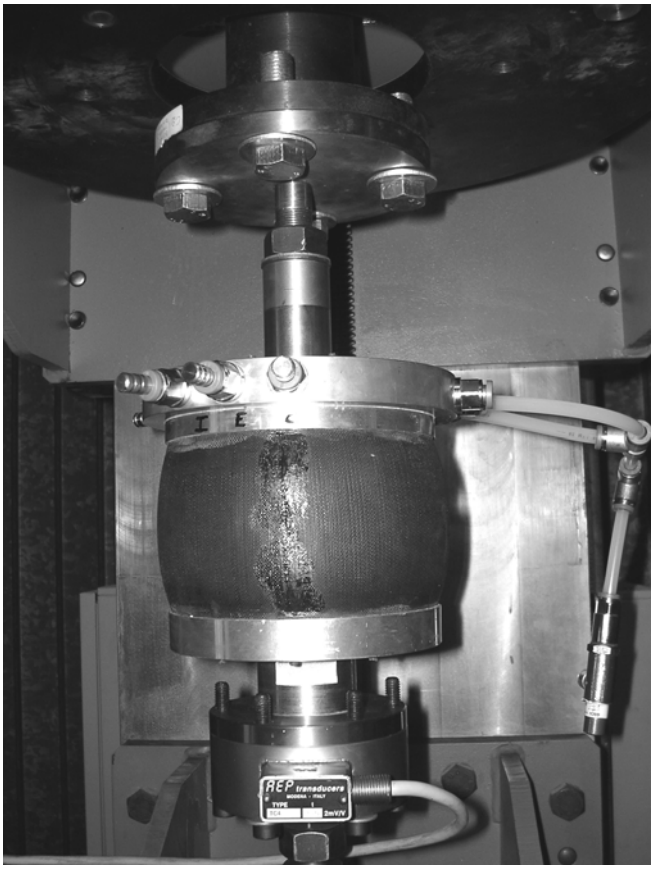

Figure 12. *BiFAc3* prototype.

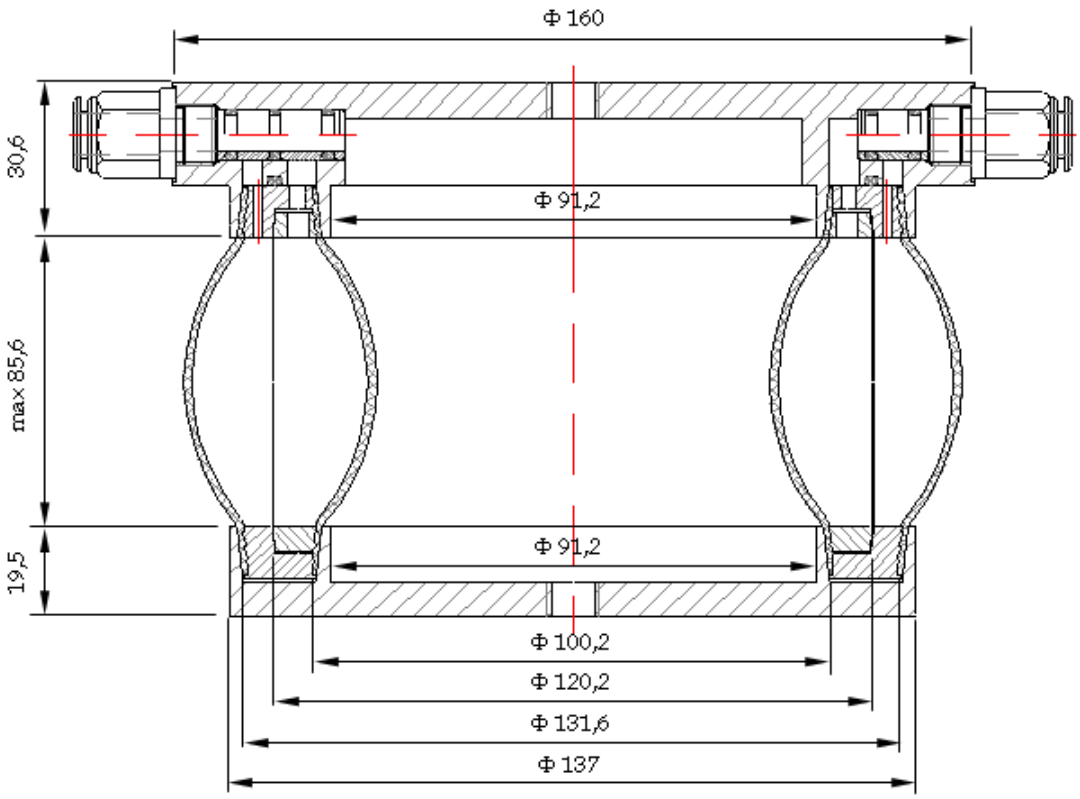

Figure 13. Cross section of the *BiFAc3* prototype.

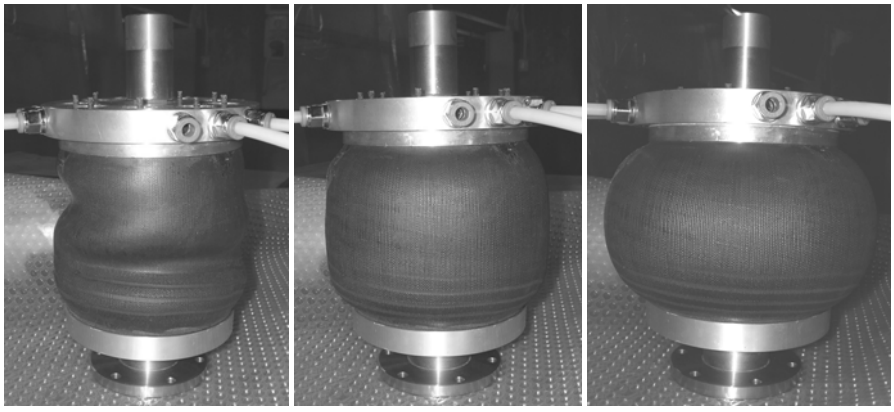

p=10 kPa **p=20 kPa** **p=60 kPa**

Figure 14. The actual shape of the membrane deformation.

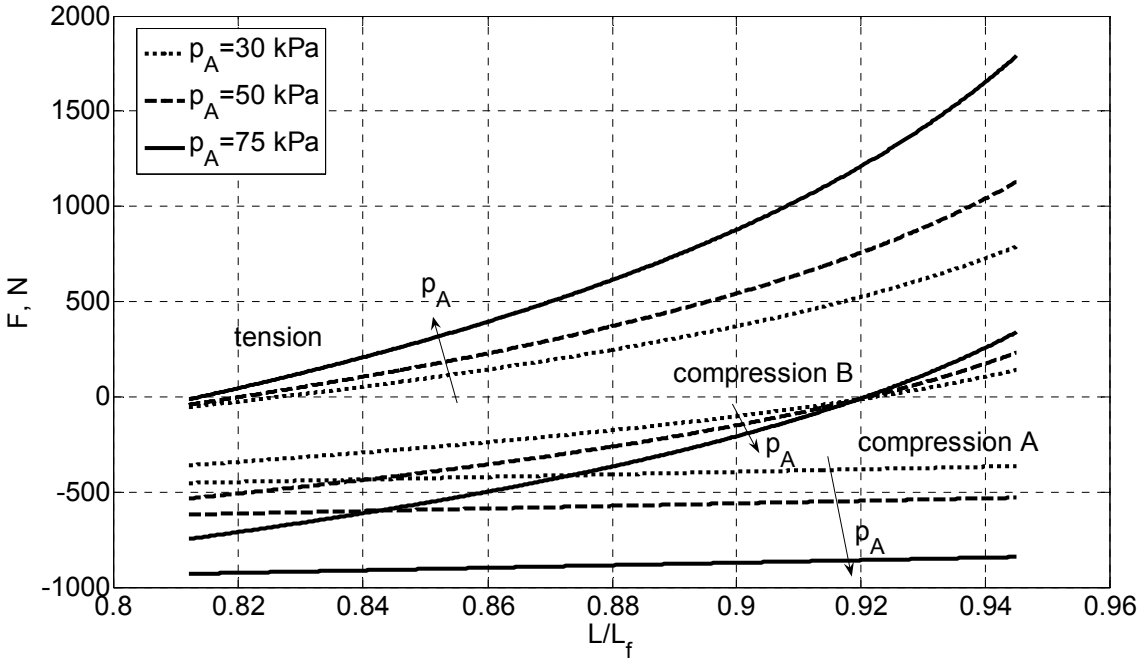

Figure 15. The static characteristic produced by the identified model.

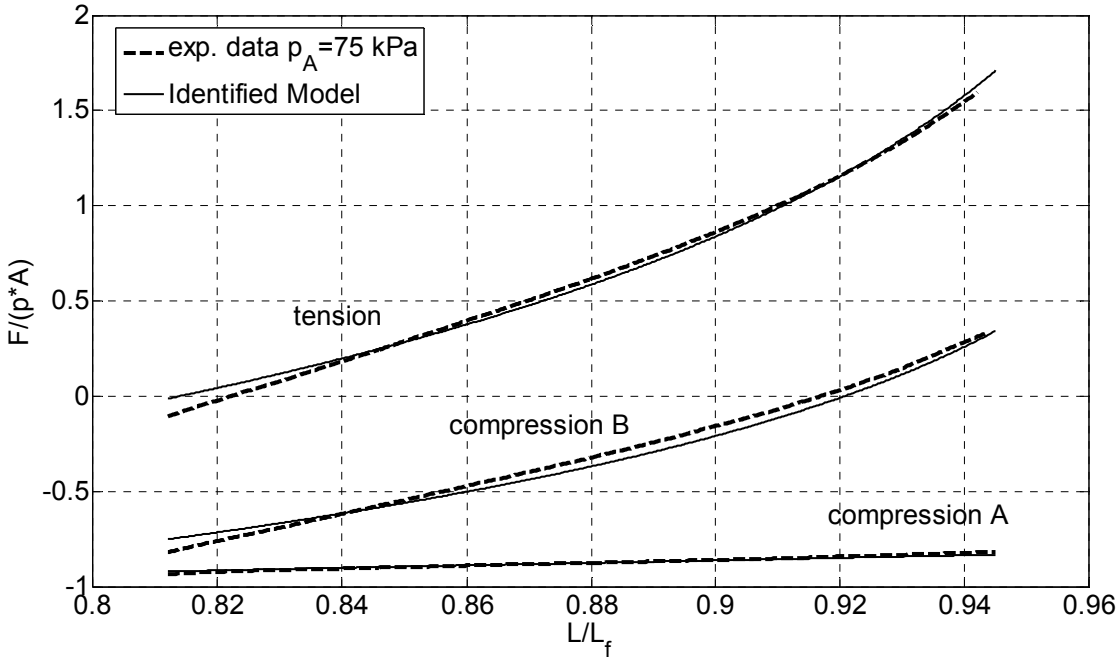

Figure 16. Comparison between the experimental and the identified model results (test stroke equal to 11 mm)